Published OnlineFirst December 13, 2017; DOI: 10.1158/1535-7163.MCT-17-0419

Small Molecule Therapeutics

Molecular Cancer Therapeutics

Antitumor Activity of Entrectinib, a Pan-TRK, ROS1, and ALK Inhibitor, in *ETV6-NTRK3*–Positive Acute Myeloid Leukemia

Kristen M. Smith[1], Patrick C. Fagan[1], Elena Pomari[2,3], Giuseppe Germano[2], Chiara Frasson[2], Colin Walsh[1], Ian Silverman[1], Paolo Bonvini[2], and Gang Li[1]

Abstract

Activation of tropomyosin receptor kinase (TRK) family tyrosine kinases by chromosomal rearrangement has been shown to drive a wide range of solid tumors and hematologic malignancies. TRK fusions are actionable targets as evidenced by recent clinical trial results in solid tumors. Entrectinib (RXDX-101) is an investigational, orally available, CNS-active, highly potent, and selective kinase inhibitor against TRKA/B/C, ROS1, and ALK kinase activities. Here, we demonstrate that TRK kinase inhibition by entrectinib selectively targets preclinical models of TRK fusion–driven hematologic malignancies. In acute myelogenous leukemia (AML) cell lines with endogenous expression of the *ETV6–NTRK3* fusion gene, entrectinib treatment blocked cell proliferation and induced apoptotic cell death *in vitro* with subnanomolar IC_{50} values. Phosphorylation of the ETV6–TRKC fusion protein and its downstream signaling effectors was inhibited by entrectinib treatment in a dose-dependent manner. In animal models, entrectinib treatment at clinically relevant doses resulted in tumor regression that was accompanied by elimination of residual cancer cells from the bone marrow. Our preclinical data demonstrate the potential of entrectinib as an effective treatment for patients with TRK fusion–driven AML and other hematologic malignancies. *Mol Cancer Ther; 17(2); 455–63. ©2017 AACR.*

Introduction

The tropomyosin receptor kinase (TRK) family receptor tyrosine kinases, TRKA, TRKB, and TRKC, are encoded by *NTRK1*, *NTRK2*, and *NTRK3* genes, respectively. Juxtaposition of 3′ *NTRK* sequences encoding the tyrosine kinase domain to various 5′ partner sequences via chromosomal rearrangement results in oncogenic TRK fusion proteins with ligand-independent constitutive kinase activation. With the use of advanced molecular diagnostic techniques, oncogenic fusions with *NTRK1*, *NTRK2*, and *NTRK3* have been identified in more than 30 tumor histologies (1–14). *NTRK* rearrangements are rare events in solid tumors, occurring with a frequency of $\leq$1% across a wide range of tumor types and more commonly in a few rare tumors (2). Recent genomic analyses of a limited number of hematopoietic tumors (15–18) suggest that *NTRK* rearrangements are likewise present at low frequencies in hematologic malignancies, including acute myelogenous leukemia (AML; refs. 1, 19, 20), chronic eosinophilic leukemia (21), B-cell acute lymphoblastic leukemia (16, 17), and multiple myeloma (18).

NTRK gene rearrangements are transforming *in vitro* and *in vivo* irrespective of the identity of the fusion partner. *TPM3-NTRK1*, *TPR-NTRK1*, and *TFG-NTRK1* gene rearrangements were originally identified in NIH3T3 cellular transformation assays (5, 12, 13). Likewise, expression of *ETV6-NTRK3*, *CD74-NTRK1*, or *MPRIP-NTRK1* transforms cell lines as evidenced by anchorage-independent growth of NIH3T3 cells and IL3-independent growth of Ba/F3 cells (9, 22, 23). Orthotopic and transgenic tumor model systems have demonstrated that *NTRK* fusion expression was sufficient for *in vivo* tumorigenesis. Transduction of primary mouse astrocytes with *TPM3-NTRK1* or *BTBD1-NTRK3*–expressing retroviruses followed by transplantation into the mouse brain generated high-grade astrocytomas with short latency and complete penetrance (6). Similar transduction and transplantation studies in the murine hematopoietic system demonstrated that *ETV6-NTRK3* expression in murine bone marrow results in a rapidly fatal myeloproliferative disease resembling AML (23). Transgenic expression of *TPR-NTRK1* under the control of a thyroid-specific promoter resulted in differentiated thyroid tumors with histologic features mirroring *NTRK* fusion–positive tumors observed in human patients (24). Finally, transgenic expression of *ETV6-NTRK3* in murine mammary epithelial cells led to rapid development of highly invasive, multifocal mammary tumors (25). These *in vitro* and *in vivo* data provide strong support that *NTRK* gene rearrangements are oncogenic driver events.

Given the central role of *NTRK* gene rearrangements in the development of numerous tumor types, inhibition of TRK kinase activity by entrectinib (26) should block the growth of these tumors. In cell lines carrying *NTRK* gene rearrangements, TRK inhibition *in vitro* by entrectinib blocked cell proliferation, induced cell-cycle arrest and apoptosis and inactivated TRK downstream signaling effectors, PLCγ, AKT, and ERK (26, 27).

[1]Ignyta, Inc., San Diego, California. [2]Foundation Institute of Pediatric Research Città della Speranza, Padova, Italy. [3]Department of Woman and Child Health, University-Hospital of Padova, Padova, Italy.

Note: Supplementary data for this article are available at Molecular Cancer Therapeutics Online (http://mct.aacrjournals.org/).

Corresponding Author: Kristen M. Smith, Ignyta, Inc., 4545 Towne Centre Court, San Diego, CA 92121. Phone: 858-255-5959; E-mail: ksmith@ignyta.com

doi: 10.1158/1535-7163.MCT-17-0419

Published OnlineFirst December 13, 2017; DOI: 10.1158/1535-7163.MCT-17-0419

The *in vivo* efficacy of entrectinib has been demonstrated against multiple preclinical *NTRK* fusion–bearing solid tumor models, including lung adenocarcinoma with an *MPRIP–NTRK1* fusion (28), colorectal carcinoma with *TPM3-NTRK1* or *LMNA-NTRK1* fusions (26, 28–30), and head and neck carcinoma with an *ETV6–NTRK3* fusion (28). Importantly, robust and durable antitumor activity has been demonstrated in patients with *NTRK*-rearranged tumors across a broad range of histologies (31).

Despite the growing body of evidence supporting therapeutic targeting of TRK in solid tumors carrying *NTRK* gene fusions, much less is known about the antitumor efficacy of TRK inhibition in liquid tumors. In this study, we examine the effect of TRK kinase inhibition in *NTRK*-rearranged patient-derived AML models.

Materials and Methods

Chemicals

Entrectinib (26), crizotinib, larotrectinib (32), and TSR-011 (33) were synthesized at Ignyta.

Cell culture

IMS-M2 and M0-91 AML cell lines were kindly provided in 2016 by Brunangelo Falini (University of Perugia, Perugia, Italy) and by Mikko Taipale (University of Toronto, Toronto, Canada), respectively, and were maintained at 37°C/5% CO_2 in RPMI/10% FBS medium as described previously (1, 34). Kasumi-1 AML cells were obtained from the ATCC in 2016 and were maintained in accordance with provided specifications. Cell line authentication and pathogen testing was performed upon receipt of cell lines (CellCheck 9 and h-IMPACT, IDEXX BioResearch). All experiments were performed on cells cultured for less than 2 months.

RNA sequencing

Total RNA was isolated using the Qiagen AllPrep Kit per the manufacturer's instructions. RNA sequencing libraries were prepared using the KAPA Stranded RNA-Seq Kit with RiboErase (HMR; KAPA Biosystems). Libraries were constructed following the manufacturer's protocol using 300 ng of total RNA. RNA was fragmented to a size of 100–200 nucleotides and amplified for 11 cycles. Final libraries were quantified on a high sensitivity bioanalyzer chip and sequenced at 1.6 pmol/L on a High Output Flowcell on the Illumina NextSeq 500. Raw FASTQ files were mapped to the human genome (hg19) with STAR (v2.5.1b_modified) aligner (35). Mapped reads were filtered and deduplicated using sambamba (v0.5.9; ref. 36). Feature quantification was performed using featureCounts (v1.5.0-p1) against the RefSeq database (downloaded from the UCSC genome browser on 03/06/2016; ref. 37). Exon-level FPKM values were determined using a custom python script. *De novo* fusion transcript identification was performed using STAR-Fusion (38), FusionAnnotator (Haas & Dobin and colleagues, https://github.com/FusionAnnotator/) and FusionInspector (Haas & Dobin and colleagues, https://github.com/FusionInspector/). RNA-Seq data was deposited in GEO under accession number GSE100885.

Cell proliferation assays

Cells were cultured in media supplemented with 10% FBS described above and seeded into 96-well microtiter plates (5,000 to 10,000 cells per well). Compounds were added in duplicate at the drug concentrations indicated using the HPD300 Digital Dispenser (Hewlett-Packard). Cells were incubated at 37°C/5% CO_2 for 72 hours and cell viability was assessed using the CellTiter Glo Luminescent Cell Viability Assay (Promega). Luminescence was measured using the ClarioSTAR plate reader (BMG). Curve-fitting and IC_{50} calculations were performed using Prism software (v6, GraphPad Software, Inc.). The mean IC_{50} values were derived from at least three independent experiments.

Immunoblot analysis

Cells were treated with entrectinib as described and whole-cell lysates were prepared in RIPA buffer containing protease and phosphatase inhibitor cocktails (Calbiochem) and benzonase (Millipore). Samples of each lysate were denatured in reducing sample buffer and loaded on 4%–12% Bis-Tris Mini-Gels in MOPS running buffer (Invitrogen). Protein was transferred to polyvinylidene difluoride membranes (Invitrogen) and immunoblotted using the following antibodies from Cell Signaling Technology: Pan-TRK (#92991), Phospho-TRKA Y674/675 (#4621), Phospho-TRKA Y785 (#4168), Phospho-TRKA Y490 (#9141), PARP (#9532), Cleaved-PARP (#5625), PLCγ (#5690), Phospho-PLCγ (#2821), Stat3 (#9139), Phospho-Stat3 (#9145), ERK (#4695), Phospho-ERK (#4377), Human CD45 (#13917), and β-Actin (#3700). Images were captured using the ChemiDoc MP Imaging System and evaluated using Image Lab 5.2.1 software (Bio-Rad).

Cell-cycle analysis

Exponentially growing cells were treated with indicated compounds for 18 hours prior to collection and fixation with 70% ethanol. Fixed cells were stained with PI/RNase staining buffer (BD Biosciences) as per the manufacturer's protocol and analyzed using a CytoFLEX flow cytometer (Beckman Coulter, Inc.). Cell-cycle phases were determined using FlowJo (v10.2, FlowJo, LLC).

Caspase-3 activation

Cells were seeded in a 96-well IncuCyte ImageLock plate (Essen Bioscience Inc.) at 10,000 cells per well 1 hour before beginning the assay. Compounds were serially diluted in DMSO and added to each well in growth media containing NucView 488 Caspase3 Substrate (2.5 μmol/L final concentration, Biotium). Assay plates were placed in an IncuCyte live-cell analysis system with a 10× objective and incubated at 37°C/5% CO_2. One image per well in both phase-contrast and fluorescence channels was collected from replicate treatment wells ($n = 6$) every 2 hours. Images were analyzed using IncuCyte ZOOM software (2016B, Essen Bioscience Inc.). Apoptotic index was calculated by dividing confluence of caspase-3 fluorescent objects by total cell confluence.

Cell morphology

Cell morphology was determined on cytospin preparations after 24-hour treatment with increasing concentrations of entrectinib. Briefly, treated and untreated 1.0×10^6 cells were harvested, washed in 1× PBS buffer, and spun (100,000 cells) onto glass slides for 8 minutes at 400 rpm using a Shandon CytoSpin3 cytocentrifuge. The cells were fixed in acetone and stained with a Wright–Giemsa solution, and images were acquired at 63× magnification with Leica DM4000B microscope and Leica DFC 420C camera (Leica Microsystem Ltd). Captured images were prepared for reproduction using dedicated software (Leica LAS V4.8 Leica Microsystems).

Published OnlineFirst December 13, 2017; DOI: 10.1158/1535-7163.MCT-17-0419

Murine *in vivo* efficacy studies

All studies were conducted in accordance with Association for Assessment and Accreditation of Laboratory Animal Care guidelines. A total of 1×10^6 tumor cells in 0.2-mL Matrigel/ RPMI (1:1 v/v, Corning) were injected subcutaneously into the right flank of 6- to 7-week-old female CB.17 SCID mice (Charles River Laboratories). Tumor dimensions were measured twice per week using Vernier calipers and tumor volume was calculated as follows: (length $\times$ width^2)/2. Animals were randomized and dosing initiated when tumor volume averaged 120–140 mm^3. Entrectinib was reconstituted in 0.5% methylcellulose (Thermo Fisher Scientific) containing 1% Tween 80 (Sigma-Aldrich). Animals were dosed daily by oral gavage with either vehicle or entrectinib at 3, 10, or 30 mg/kg as indicated. Biweekly body weight measurements were conducted to monitor toxicity. Entrectinib treatment was terminated and all mice euthanized when the vehicle-treated group reached 2,000 mm^3. Bone marrow cells were harvested by flushing femurs with ice-cold PBS. Live cells were identified using the LIVE/DEAD Fixable Near-IR Stain Kit (Thermo Fisher Scientific), blocked with mouse FcR Blocking Reagent (Miltenyi Biotec) and stained with the following antibodies to identify human AML cells: anti-human CD45 (clone HI30, BioLegend), anti-mouse CD45 (clone 30-F11, BD Biosciences), anti-human CD33 (clone P67.6, BioLegend), anti-human CD34 (clone 581, BD Biosciences), and anti-human CD38 (clone HB-7, BioLegend). For biomarker modulation studies presented in Fig. 3C, additional tumor-bearing mice (n = 3/group, tumor volumes of 300–500 mm^3) were dosed orally with vehicle or entrectinib at 3 or 30 mg/kg as indicated. Mice were euthanized 4 hours post single dose administration. Tumors were harvested and flash-frozen in liquid nitrogen for immunoblot analysis as described above. Tumor lysates were prepared in RIPA buffer containing protease and phosphatase inhibitor cocktails (Calbiochem) and benzonase (Millipore) using FastPrep 24 System (MP Biomedicals).

Zebrafish *in vivo* efficacy studies

Zebrafish were mated, staged and raised as described previously (39) and maintained according to the OPBA of the Istituto di Ricerca Pediatrica guidelines. Wild-type AB strain zebrafish embryos were dechorionated manually 24 hours postfertilization (hpf) and maintained into E3 medium with 0.3% phenylthiourea (Sigma-Aldrich) added to inhibit melanization. To test compound toxicity, 72 hpf zebrafish embryos (n = 30) were placed in a 6-well plate (n = 10/well) containing 1 mL E3 media, in which entrectinib was diluted at 50 nmol/L, 500 nmol/L, 1 μmol/L, or 2 μmol/L. Embryos were monitored daily for 3 days with fresh medium added daily. Entrectinib treatment did not significantly alter embryo survival under these conditions (Supplementary Fig. S6B and S6C). For xenotransplantation experiments, 48 hpf embryos were anesthetized with 0.003% tricaine (Sigma-Aldrich) and positioned on a wet 2% agarose petri dish. Cells were labeled with CM-Dil (Thermo Fisher Scientific) per the manufacturer's instructions before injection into 48 hpf zebrafish embryos. Approximately 300–400 labeled cells were injected into the duct of Cuvier of each embryo using an automated injector (Nanoject II, Drummond Scientific) equipped with borosilicate glass capillaries. Injected embryos were maintained at 28°C for 1 hour and then at 34°C for the successive 24 hours. Embryos with similar red fluorescence cells in the caudal part were moved to 6-well plates (40 embryo/well) containing entrectinib diluted into 2-mL E3 media or treated with DMSO (0.1% (v/v) as negative control. All embryos were subsequently maintained at 34°C. Brightfield and fluorescence imaging of the embryos was performed with a Nikon SMZ1500 stereoscope equipped with Nikon Digital Sight and NIS25 Elements 4.0 software. Tumor xenografts were evaluated 24 or 48 hours posttreatment (hpt) by flow cytometry. Embryos (30–35 per treatment) were anesthetized with 0.003% tricaine (Sigma-Aldrich) and pooled to generate cell suspensions. Cells were stained with PE-conjugated anti-CD33 antibody (Beckman Coulter, Inc.) and analyzed with a Cytomics FC 500 system (Beckman Coulter, lnc.) to detect CM-DiI$^+$/CD33$^+$ cells. As a negative control, CM-DiI and CD33 fluorescence was measured in noninjected embryos at 72 and 96 hpf to exclude any cross-species detection between human and zebrafish cells.

Results

Two AML cell lines carrying *NTRK* fusion genes were identified. IMS-M2 was established from a 59-year-old patient with FAB M2 AML (1), whereas M0-91 was established from a patient with FAB M0 AML (40). We confirmed that both cell lines express hematopoietic and myeloid cell surface markers, including CD45 and CD33 (Supplementary Fig. S1), and verified the presence of an *ETV6–NTRK3* fusion by Trailblaze Pharos assay (41) and/or RNA-Seq. Exons 1–4 of *ETV6* were fused in-frame to *NTRK3* exon 15 (Fig. 1A and B) in both cell lines. In comparison, *ETV6–NTRK3* fusions identified in solid tumors result from in-frame fusion of *ETV6* exons 1–5 to *NTRK3* exon 14 or 15, or *ETV6* exons 1–4 fused to *NTRK3* exon 14 (diagram in Fig. 1A; refs. 4, 42). Fusions of *ETV6* exon 5 to *NTRK3* exon 15 have also been described in AML, acute lymphoid leukemia, and chronic eosinophilic leukemia (16, 20, 21). Although *NTRK3* exons 15–20 were expressed in IMS-M2 and M0-91 cells, no expression from exons 5′ of *NTRK3* exon 15 was observed (Fig. 1B), confirming previous observations that full-length *NTRK3* mRNA is not expressed in these cell lines. mRNA expression of *NTRK1* was detected in both cell lines (Fig. 1B); however, *NTRK2*, *ALK*, and *ROS1* expression was either absent or observed at extremely low levels and no expression of TRK ligands, NGF, NT3, NT4, or BDNF, was observed (Supplementary Fig. S1C). Furthermore, next-generation sequencing targeting exons of 265 cancer genes did not identify additional oncogenic driver mutations in the IMS-M2 and M0-91 cells. Taken together, these data suggest that *ETV6-NTRK3* is the oncogenic driver in both IMS-M2 and M0-91 cell lines.

We evaluated the *in vitro* antiproliferative activity of entrectinib against IMS-M2, M0-91 and Kasumi-1, a FAB M2 AML-derived cell line carrying the *RUNX1-RUNX1T1* (*AML1-ETO*) translocation (43). We compared entrectinib antiproliferative activity to crizotinib, a c-MET/ALK/ROS1 tyrosine kinase inhibitor as well as two additional compounds with TRK inhibitor ability, larotrectinib (LOXO-101) and TSR-011 (Fig. 1C and D). Entrectinib inhibited IMS-M2 and M0-91 cellular proliferation at subnanomolar concentrations (0.47 and 0.65 nmol/L, respectively) while having no effect on Kasumi-1 cells at physiologically relevant concentrations (Fig. 1C). Entrectinib was 6.4- to 158-fold more potent than other tested tyrosine kinase inhibitors (Fig. 1D).

To confirm TRK kinase targeting following entrectinib treatment, IMS-M2 or M0-91 cells were treated with serial dilutions of entrectinib *in vitro* and cell lysates were examined by immunoblotting. Tyrosine phosphorylation of ETV6–TRKC on the kinase

Published OnlineFirst December 13, 2017; DOI: 10.1158/1535-7163.MCT-17-0419

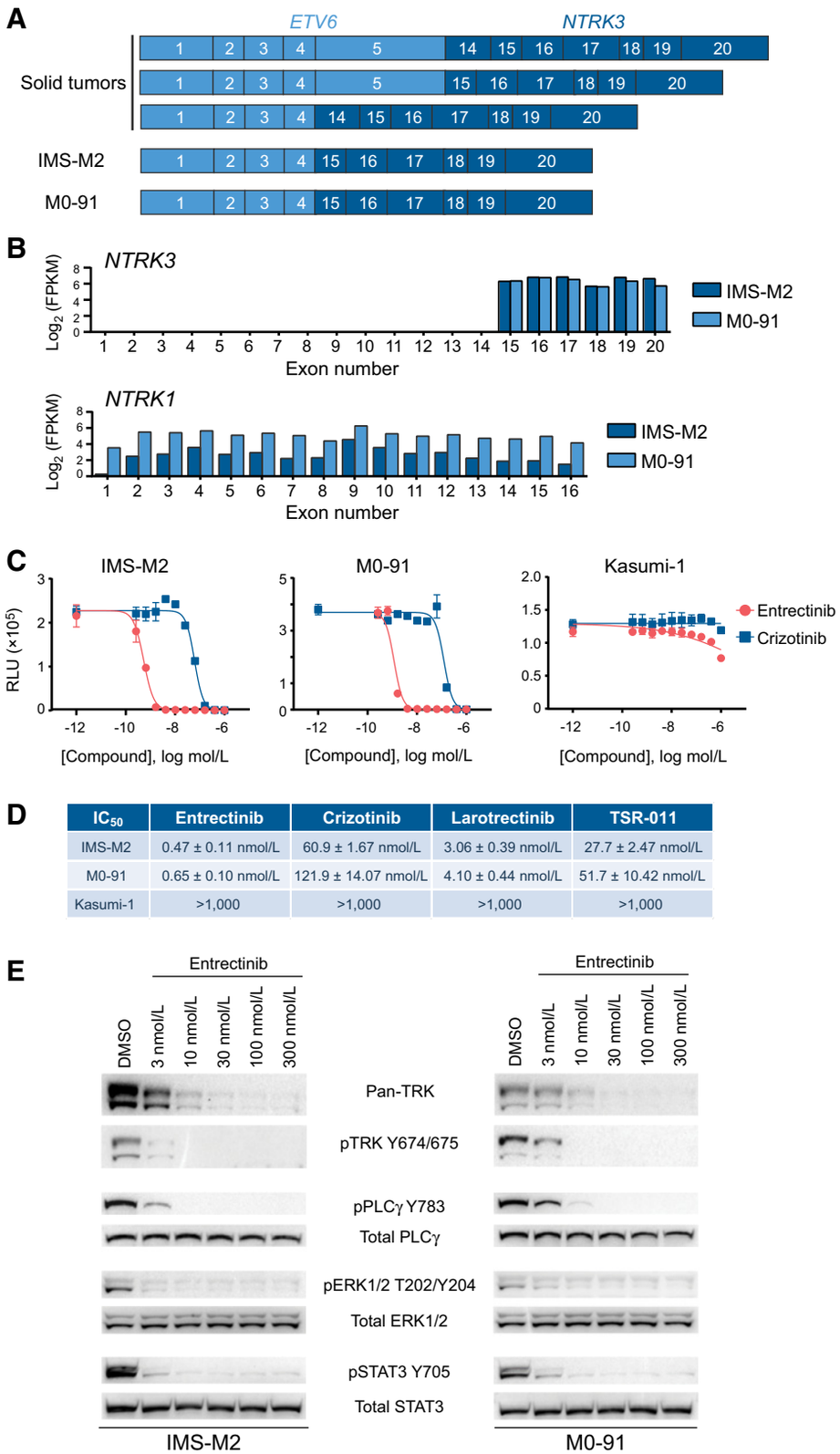

IC_{50}	Entrectinib	Crizotinib	Larotrectinib	TSR-011
IMS-M2	0.47 ± 0.11 nmol/L	60.9 ± 1.67 nmol/L	3.06 ± 0.39 nmol/L	27.7 ± 2.47 nmol/L
M0-91	0.65 ± 0.10 nmol/L	121.9 ± 14.07 nmol/L	4.10 ± 0.44 nmol/L	51.7 ± 10.42 nmol/L
Kasumi-1	>1,000	>1,000	>1,000	>1,000

Figure 1.

In vitro entrectinib treatment potently inhibits cellular proliferation and TRK signaling in *ETV6-NTRK3*–driven AML cell lines. **A,** Diagram of *ETV6–NTRK3* fusions identified in solid tumors (4, 42), IMS-M2, and M0-91 cell lines. Exon numbering is based on NM_001012338 (*NTRK3*) and NM_001987 (*ETV6*) reference sequences. **B,** Exon-level quantification of *NTRK3* (top) and *NTRK1* (bottom) expression for IMS-M2 and M0-91 determined by RNA sequencing. Exon numbering based on NM_001012338 (*NTRK3*) and NM_001012331 (*NTRK1*) reference sequences. FPKM, Fragments per kilobase of transcript per million reads mapped. **C,** Cell viability was measured using the CellTiter-Glo viability assay following 72-hour treatment with serial dilutions of entrectinib (red line) or crizotinib (blue line). The IC_{50} value was determined using 4-parameter curve fit (Prism). Bars indicate SEM. A representative of three independent experiments is shown. **D,** Summary of cell viability experiments (mean ± SEM, $n = 3$). Entrectinib was several orders of magnitude more potent than other TRK, ROS, or ALK inhibitors tested. Little or no growth-inhibitory effect was observed in the nonfusion AML cell line Kasumi-1. **E,** IMS-M2 (left) or M0-91 (right) cells were treated with entrectinib for 2 hours at the indicated concentrations. Whole-cell lysates were immunoblotted with anti-pan-TRK, anti-phospho-TRK Y674/675, or key targets in the downstream TRK signaling pathways as indicated. Rapid and sustained decreases were observed in phosphorylation of TRK, PLCγ (Y783), ERK 1/2 (T202/Y204), and STAT3 (Y705) in both *ETV6-NTRK3*–positive cell lines. Results from a representative experiment are shown.

Published OnlineFirst December 13, 2017; DOI: 10.1158/1535-7163.MCT-17-0419

domain activation loop (pTRK Y764/Y765, Fig. 1E) and the PLCγ interaction site (pTRK Y785, Supplementary Fig. S2) was reduced in a dose-dependent manner. ETV6–TRKC protein appeared to be rapidly degraded upon entrectinib treatment, mirroring the decrease in TRK tyrosine phosphorylation (Fig. 1E). Phosphorylation of TRKC downstream signaling components, PLCγ, ERK1/2, and STAT3, was also inhibited in a dose-dependent manner (Fig. 1E).

Entrectinib treatment at low nanomolar doses resulted in cell death in IMS-M2 and M0-91 cell lines. IMS-M2 cells underwent a G_1 cell-cycle arrest at doses of entrectinib at or above 1 nmol/L, while doses above 3 nmol/L also increased the sub-G_1 cell population (Fig. 2A). Likewise, entrectinib induced cell death in M0-91 cells in a dose-dependent manner with a majority of the cells having sub-G_1 DNA content at doses at or above 10 nmol/L (Fig. 2A). Entrectinib treatment induced apoptotic cell death as evidenced by caspase-3 activation (Fig. 2B; Supplementary Fig. S3), PARP cleavage (Fig. 2C), and cell shrinkage and chromatin condensation (Fig. 2D) in a time- and dose-dependent manner. Overall, these data demonstrate that entrectinib treatment specifically inhibits *in vitro* proliferation and survival of *ETV6–NTRK3* fusion–positive AML cell lines.

To test the *in vivo* efficacy of entrectinib, we treated mice with subcutaneous xenograft tumors daily with vehicle or entrectinib. Entrectinib treatment at either 10 or 30 mg/kg resulted in complete regression of both IMS-M2 and M0-91 xenograft tumors while 3 mg/kg significantly inhibited tumor growth (Fig. 3A and B). No significant differences in body weights between treatment groups were observed (Supplementary Fig. S4). The dose-dependent effect of entrectinib on tumor growth inhibition was paralleled by a dose-dependent decrease in phosphorylation of ETV6–TRKC and TRK downstream signaling components (Fig. 3C). To assess biomarker modulation by entrectinib, additional IMS-M2 or M0-91 tumor-bearing mice were treated with a single dose of vehicle, entrectinib at 3 mg/kg or entrectinib at 30 mg/kg for 4 hours. This time point was chosen based on reported murine pharmacokinetics (26). ETV6–TRKC phosphorylation, as well as total ETV6–TRKC protein, was reduced with a single 3 mg/kg dose and eliminated with a 30 mg/kg dose of entrectinib. PLCγ, ERK1/2, and STAT3 phosphorylation was substantially reduced upon entrectinib treatment with no observed alteration in PLCγ, ERK1/2, and STAT3 total protein amount. Immunoblots for human CD45 were performed to confirm human xenografts and to demonstrate equivalent protein loading across treated samples.

We next examined the effect of entrectinib treatment on leukemic cells in orthotopic sites. AML tumor cells spontaneously migrate to the bone marrow in mice bearing subcutaneous IMS-M2 xenograft tumors. To determine whether IMS-M2 tumor cells in the bone marrow were sensitive to entrectinib, we harvested bone marrow from IMS-M2 tumor-bearing mice after 3 weeks of daily treatment with vehicle or entrectinib (3, 10, or 30 mg/kg) and determined the percentage of human CD45-positive cells by flow cytometry. We confirmed that human CD45-positive cells found in the bone marrow also expressed CD33 and lacked expression of murine CD45 (Supplementary Fig. S5A). No human CD45-positive cells could be detected following entrectinib treatment, whereas all vehicle-treated mice had a distinct human CD45-positive cell population in the bone marrow (Fig. 3D; Supplementary Fig. S5B).

M0-91 cells did not exhibit bone marrow homing from subcutaneous tumors, so we performed zebrafish xenotransplantation studies to examine the orthotopic efficacy of entrectinib against this cell line. Xenotransplantation of human cancer cells into zebrafish has emerged as a powerful model to study preclinical therapeutics efficacy, using both cell lines and primary tumor cells (44). CM-DiI–labeled M0-91 cells were injected into the duct of Cuvier space of 2-days post-fertilization (dpf) zebrafish embryos. We injected 400 cells per embryo and monitored labeled human cells in circulation for up to 4 days, an adequate window for drug screening (Supplementary Fig. S6A). Transplanted embryos were confirmed by fluorescence microscopy (Fig. 3E) and analyzed 24 and 48 hours post treatment (hpt) with 0.5 μmol/L or 1 μmol/L entrectinib. Under these conditions, M0-91 cells were sensitive to entrectinib treatment with the number of CM-Dil–labeled CD33-positive cells quantified by flow cytometry decreasing in both a time- and dose-dependent manner without apparent toxic effects (Fig. 3F).

Discussion

TRK kinase inhibition by entrectinib has emerged as a viable treatment option for patients with solid tumors carrying *NTRK* gene fusions, as demonstrated by its *in vitro* and *in vivo* antitumor efficacy in multiple preclinical *NTRK* fusion-bearing solid tumor models (26, 28–30), and by the robust clinical responses in patients with *NTRK*-rearranged tumors observed across a broad range of solid tumors and independent of 5′ fusion partner (31). Here we demonstrated that the TRK kinase inhibition by entrectinib was similarly efficacious in preclinical AML models harboring an *NTRK* gene fusion.

AML is the most common form of acute leukemia in adults and is a heterogenous disease with wide variation in clinical response. Only 35%–40% of adult AML patients respond to the current standard-of-care therapy, consisting of intensive induction anthracycline and cytarabine chemotherapy followed by hematopoietic stem cell transplant consolidation where appropriate. Reflective of the variability in clinical response, AML is genetically diverse with recurrent driver alterations identified across more than 70 genes or genomic regions (15, 45). However, a significant percentage of patients do not have identified molecular alterations in these canonical drivers (15). Recent advances in molecular diagnostics have enabled the search for additional actionable alterations within this group of patients.

The *ETV6–NTRK3* fusion gene is one such oncogenic driver identified in AML (1, 19, 20), as expression of ETV6–TRKC is sufficient to drive myeloid leukemogenesis in preclinical models (23). Various *ETV6–NTRK3* fusion breakpoints have been identified in clinical samples including *ETV6* exon 4 fused to *NTRK3* exons 14 or 15 (e4-e14, e4-e15) and *ETV6* exon 5 fused to *NTRK3* exons 14 or 15 (e5-e14, e5-e15; diagram in Fig. 1A). All identified fusions are transforming *in vitro* (3, 22, 23, 46) and all are sensitive to entrectinib with nanomolar or subnanomolar IC_{50} values in 72-hour proliferation assays (0.37 nmol/L for e4-e14, 0.47–0.65 nmol/L for e4–e15 and 4.47 nmol/L for e5–e15 fusions; this study and ref. 46).

Entrectinib treatment potently blocked cellular proliferation in *NTRK* fusion–positive AML patient-derived cell lines (Fig. 1C) and resulted in rapid apoptotic cell death in a dose- and time-dependent manner (Fig. 2). Cell death was preceded by rapid reduction in TRK autophosphorylation at Y764/Y765 in the kinase activation loop and Y785, the PLCγ interaction site, and by reduced phosphorylation of downstream signaling partners,

Published OnlineFirst December 13, 2017; DOI: 10.1158/1535-7163.MCT-17-0419

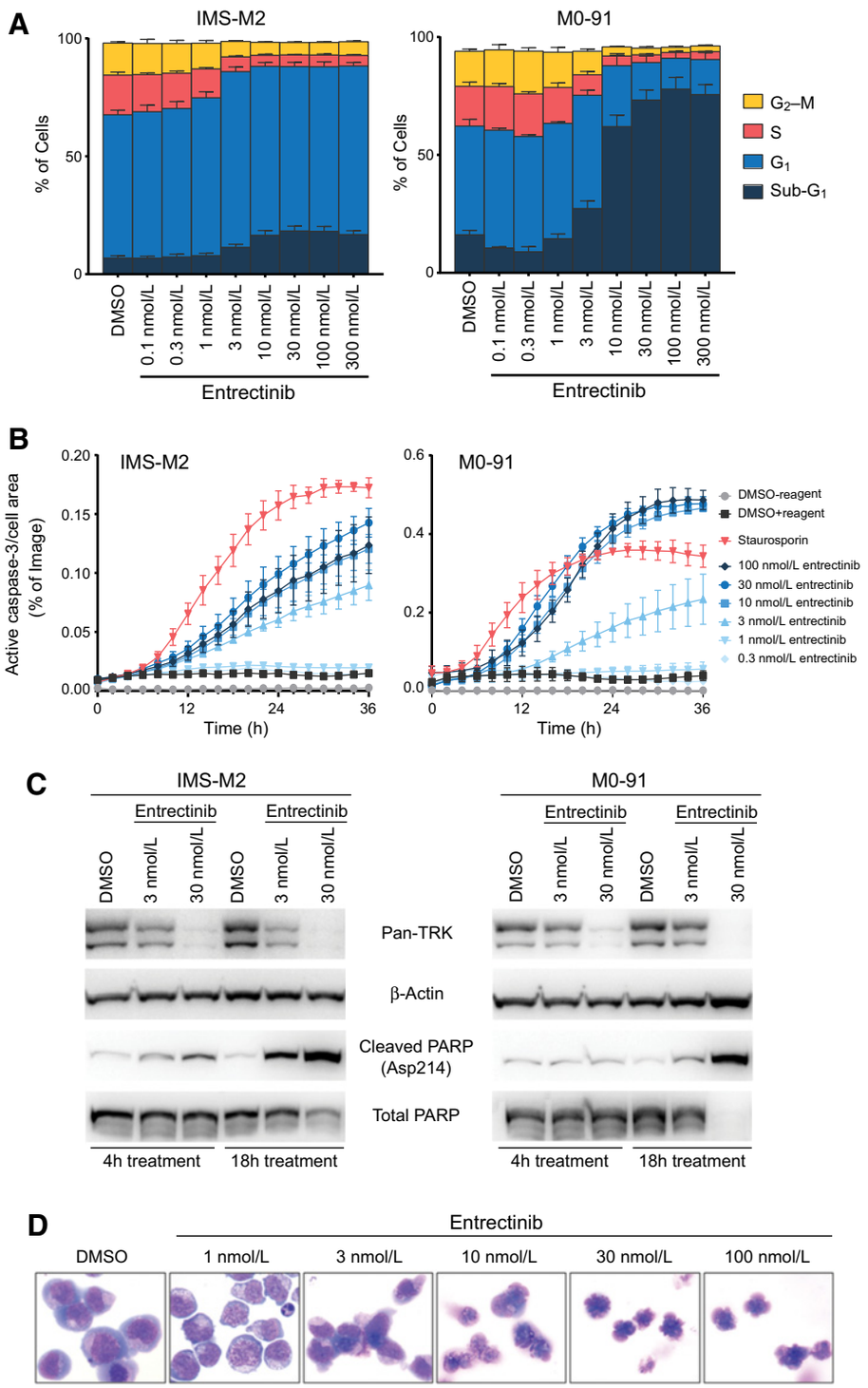

Figure 2.

Entrectinib treatment rapidly induces apoptosis in *ETV6-NTRK3*–driven AML cell lines. **A,** Flow cytometric analysis of cell-cycle progression in *NTRK* fusion–positive AML cell lines treated with entrectinib for 18 hours. Columns depict average ± SEM of three independent experiments. **B,** Time-lapse image analysis showed entrectinib dose-dependent caspase-3 activation in IMS-M2 (left) or M0-91 (right) cells. Cells were treated with serial dilutions of entrectinib in the presence of NucView 488 Caspase-3 Substrate and imaged every 2 hours. Treatment with 500 nmol/L staurosporin served as a positive control. Average ± SEM of three independent experiments is shown. **C,** IMS-M2 or M0-91 cells were treated with DMSO or entrectinib (3 or 30 nmol/L) for 4 or 18 hours. Whole-cell lysates were immunoblotted with anti-pan-TRK, anti-cleaved PARP, or anti-total PARP. Extracts were equally loaded as determined by anti-β-actin immunoblotting. Elevated PARP cleavage was observed in IMS-M2 and M0-91 cell lines as early as 4 hours and reached maximal levels by 18 hours following exposure to entrectinib. Results from a representative experiment are shown. **D,** Representative images of Wright-Giemsa–stained cytospin preparations of M0-91 cells treated with indicated concentrations of entrectinib; original magnification, ×63.

PLCγ, ERK, and STAT3 (Fig. 1E and F). TRK kinase inhibition was also accompanied by a reduction in ETV6–TRKC fusion protein levels (Fig. 1F). Similar reductions in PML–RARA fusion protein stability after retinoic acid/arsenic trioxide treatment or estrogen receptor after fulvestrant treatment (47, 48) have been described. Altered protein stability upon entrectinib treatment may be a novel mechanism of action against TRKC fusion proteins as reduced TRK fusion protein levels have not been seen after entrectinib treatment of patient-derived cell lines carrying TRKA fusions or Ba/F3 cells expressing *ETV6–NTRK1* (26).

Both IMS-M2 and M0-91 cell lines had remarkably similar responses to entrectinib treatment *in vitro* and *in vivo*. Importantly,

Published OnlineFirst December 13, 2017; DOI: 10.1158/1535-7163.MCT-17-0419

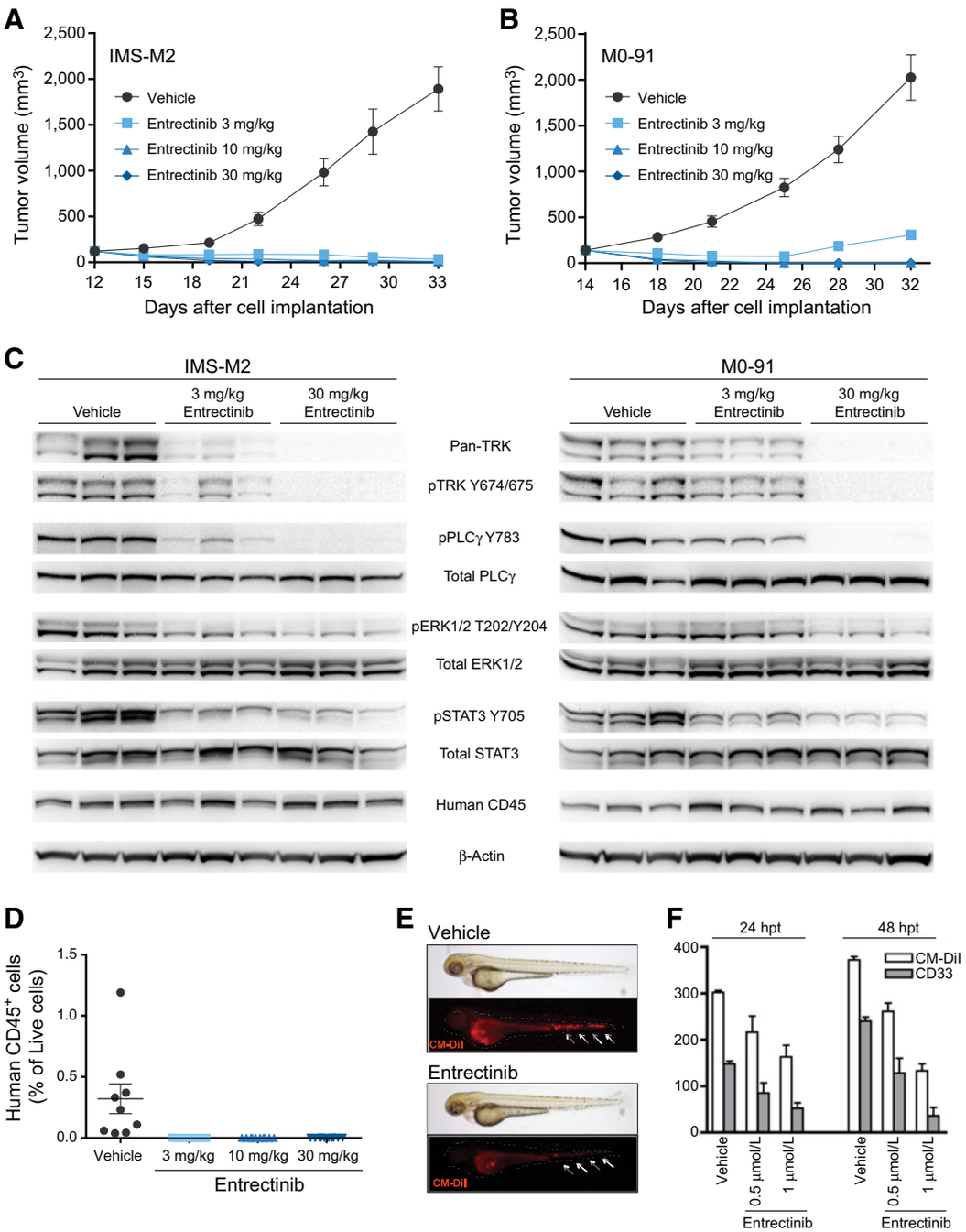

Figure 3.

Entrectinib treatment results in xenograft tumor regression and effective targeting of *ETV6-NTRK3*–driven AML cell lines. CB.17 SCID mice bearing subcutaneous IMS-M2 (**A**) or M0-91 (**B**) xenograft tumors were administered vehicle or entrectinib at the indicated doses daily. Tumor volume for each group was measured twice weekly. Data are expressed as mean ± SEM (n = 9–10/ group). **C,** Dose-dependent inhibition of TRK, PLCγ, ERK, and STAT3 phosphorylation in tumor lysates prepared from tumor-bearing mice treated with a single dose of vehicle or entrectinib (3 or 30 mg/kg, n = 3/group) and collected 4 hours postdosing. Tumor lysates from 3 individual tumor-bearing mice are shown per treatment condition. **D,** Flow cytometric analysis of bone marrow from IMS-M2 tumor-bearing mice after 21 days of treatment with vehicle or entrectinib (3, 10, or 30 mg/kg). The mean percentage of live human CD45-positive, mouse CD45-negative cells is indicated (n = 9–10 mice/group); bars indicate SEM. The gating strategy is described in Supplementary Fig. S6. **E,** Representative bright field and fluorescent images of xenotransplanted zebrafish embryos at 24 hours posttreatment (hpt) with 1 mmol/L entrectinib or DMSO vehicle. White arrows indicate human CM-DiI–positive M0-91 leukemic cells disseminated in the circulation system from the injection site (duct of Cuvier). **F,** CM-DiI M0-91 cells analysis from xenotransplanted zebrafish embryos after treatment with entrectinib at the indicated dosages. Fluorescent M0-91 cells were detected by flow cytometry and assessed for the expression of human CD33 antigen as indicated.

we also demonstrated that entrectinib treatment targeted AML cells in orthotopic sites, including the bone marrow of tumor-bearing mice and the circulation of transplanted zebrafish. However, subtle differences between the cell lines were noted. IMS-M2 cells were overall more sensitive to entrectinib treatment with an IC_{50} value of 0.47 nmol/L versus 0.65 nmol/L for M0-91 cells in *in vitro* proliferation assays. This slight difference in sensitivity was also observed when TRK, PLCγ, ERK, or STAT3 protein phosphorylation was examined after treatment with serial dilutions of entrectinib (Figs. 1E and F and 3C). *In vivo*, IMS-M2 xenograft tumor growth was fully inhibited even at the lowest tested dose (3 mg/kg), whereas limited tumor proliferation was seen in M0-91 xenograft tumors at the same dose. The incomplete tumor growth inhibition is likely due to incomplete drug dosing of M0-91 tumors as similar tumor growth was seen in all cohort animals and tumors treated with 3 mg/kg remained responsive to higher doses of entrectinib. Finally, there were differences in the apoptotic cell death response. IMS-M2 cells exhibited a G_1 arrest phenotype in response to entrectinib followed by apoptotic cell death. At 18 hours post-entrectinib treatment, 15%–20% of IMS-M2 cells were apoptotic as shown by sub-G_1 DNA content and by the percentage of apoptotic cells continuing to increase over 36 hours (Fig. 2A and B). In contrast, entrectinib treatment of M0-91 cells resulted in rapid apoptotic changes with no evidence of cell-cycle arrest. Both cell lines were exquisitely sensitive to entrectinib; however, understanding the subtle differences between these cell lines may provide useful insights into *ETV6–NTRKC*–dependent oncogenesis.

Although this study examines the efficacy of entrectinib against *ETV6–NTRK3* fusion–positive AML, these results are likely to be applicable to other hematologic malignancies. In addition to AML, *NTRK* gene fusions have been identified in Philadelphia chromosome–like B-cell acute lymphoid leukemia (16, 17), chronic eosinophilic leukemia (21), and multiple myeloma (18). Analyses of a limited number of patients (15–18) suggest that *NTRK* fusion prevalence in hematologic malignancies is $\leq$1%. This frequency is similar to solid tumor biology where *NTRK* fusions are rare events across a wide range of tumor histologies (2). As the incidence of molecular tumor profiling increases in hematopoietic malignancies, it is increasingly important to investigate therapeutic options for patients with rare but actionable alterations such as *NTRK* fusions. Entrectinib is currently being studied in a phase II clinical trial (NCT02568267: "STARTRK-2") and a pediatric clinical trial (NCT02650401: "STARTRK-NG") for patients with solid tumors harboring *NTRK*, *ROS1*, or *ALK* gene fusions. Phase I studies demonstrated that entrectinib was well tolerated and generated durable clinical responses in patients with *NTRK* fusion–positive solid tumors independent of tumor type or fusion partner (31). Given the positive clinical evidence observed in solid tumors and our preclinical data described here, entrectinib has the potential to be a promising agent for the treatment of hematologic malignancies with evidence of TRK activation.

Disclosure of Potential Conflicts of Interest

No potential conflicts of interest were disclosed.

Authors' Contributions

Conception and design: K.M. Smith, P.C. Fagan, G. Germano, P. Bonvini, Gang Li

Development of methodology: K.M. Smith, P.C. Fagan, C. Walsh

Acquisition of data (provided animals, acquired and managed patients, provided facilities, etc.): K.M. Smith, P.C. Fagan, G. Germano, C. Frasson, C. Walsh

Analysis and interpretation of data (e.g., statistical analysis, biostatistics, computational analysis): K.M. Smith, P.C. Fagan, E. Pomari, G. Germano, C. Walsh, I. Silverman

Writing, review, and/or revision of the manuscript: K.M. Smith, P.C. Fagan, E. Pomari, G. Germano, I. Silverman, P. Bonvini, Gang Li

Administrative, technical, or material support (i.e., reporting or organizing data, constructing databases): K.M. Smith, P.C. Fagan, C. Walsh

Study supervision: K.M. Smith, P. Bonvini, Gang Li

Acknowledgments

We thank Maria Barrerra for technical assistance with *in vivo* assays and Roopal Patel and Gina Wei for helpful discussions. We would also like to thank Gina Wei for critical review of this article. This work was financially supported by Ignyta, Inc. P. Bonvini and C. Frasson are supported by Fondazione Istituto di Ricerca Pediatrica Città della Speranza (Padova, Italy). C. Frasson is supported by Azienda Ospedaliera of Padova (Padova, Italy).

The costs of publication of this article were defrayed in part by the payment of page charges. This article must therefore be hereby marked *advertisement* in accordance with 18 U.S.C. Section 1734 solely to indicate this fact.

Received May 8, 2017; revised July 10, 2017; accepted November 21, 2017; published OnlineFirst December 13, 2017.

References

1. Eguchi M, Eguchi-Ishimae M, Tojo A, Morishita K, Suzuki K, Sato Y, et al. Fusion of ETV6 to neurotrophin-3 receptor TRKC in acute myeloid leukemia with t(12;15)(p13;q25). Blood 1999;93:1355–63.
2. Stransky N, Cerami E, Schalm S, Kim JL, Lengauer C. The landscape of kinase fusions in cancer. Nat Commun 2014;5:4846.
3. Tognon C, Knezevich SR, Huntsman D, Roskelley CD, Melnyk N, Mathers JA, et al. Expression of the ETV6-NTRK3 gene fusion as a primary event in human secretory breast carcinoma. Cancer Cell 2002;2:367–76.
4. Knezevich SR, McFadden DE, Tao W, Lim JF, Sorensen PH. A novel ETV6-NTRK3 gene fusion in congenital fibrosarcoma. Nat Genet 1998;18:184–7.
5. Martin-Zanca D, Hughes SH, Barbacid M. A human oncogene formed by the fusion of truncated tropomyosin and protein tyrosine kinase sequences. Nature 1986;319:743–8.
6. Wu G, Diaz AK, Paugh BS, Rankin SL, Ju B, Li Y, et al. The genomic landscape of diffuse intrinsic pontine glioma and pediatric non-brainstem high-grade glioma. Nat Genet 2014;46:444–50.
7. Yoo SK, Lee S, Kim S, Jee HG, Kim BA, Cho H, et al. Comprehensive analysis of the transcriptional and mutational landscape of follicular and papillary thyroid cancers. PLoS Genet 2016;12:e1006239.
8. Frattini V, Trifonov V, Chan JM, Castano A, Lia M, Abate F, et al. The integrated landscape of driver genomic alterations in glioblastoma. Nat Genet 2013;45:1141–9.
9. Vaishnavi A, Capelletti M, Le AT, Kako S, Butaney M, Ercan D, et al. Oncogenic and drug sensitive NTRK1 rearrangements in lung cancer. Nat Med 2013;19:1469–72.
10. Skálová A, Vanecek T, Sima R, Laco J, Weinreb I, Perez-Ordoñez B, et al. Mammary analogue secretory carcinoma of salivary glands, containing the ETV6-NTRK3 fusion gene: a hitherto undescribed salivary gland tumor entity. Am J Surg Pathol 2010;34:599–608.
11. Farago AF, Le LP, Zheng Z, Muzikansky A, Drilon A, Patel M, et al. Durable clinical response to entrectinib in NTRK1-rearranged non–small cell lung cancer. J Thorac Oncol 2015;10:1670–4.
12. Greco A, Pierotti M, Bongarzone I, Pagliardini S, Lanzi C, Della Porta G. TRK-T1 is a novel oncogene formed by the fusion of TPR and TRK genes in human papillary thyroid carcinomas. Oncogene 1992;7:237–42.
13. Greco A, Mariani C, Miranda C, Lupas A, Pagliardini S, Pomati M, et al. The DNA rearrangement that generates the TRK-T3 oncogene involves a novel

gene on chromosome 3 whose product has a potential coiled-coil domain. Mol Cell Biol 1995;15:6118–27.
14. Jones DT, Hutter B, Jäger N, Korshunov A, Kool M, Warnatz HJ, et al. Recurrent somatic alterations of FGFR1 and NTRK2 in pilocytic astrocytoma. Nat Genet 2013;45:927–32.
15. Papaemmanuil E, Gerstung M, Bullinger L, Gaidzik VI, Paschka P, Roberts ND, et al. Genomic classification and prognosis in acute myeloid leukemia. N Engl J Med 2016;374:2209–21.
16. Roberts KG, Li Y, Payne-Turner D, Harvey RC, Yang YL, Pei D, et al. Targetable kinase-activating lesions in Ph-like acute lymphoblastic leukemia. N Engl J Med 2014;371:1005–15.
17. Roberts KG, Gu Z, Payne-Turner D, McCastlain K, Harvey RC, Chen IM, et al. High frequency and poor outcome of philadelphia chromosome–like acute lymphoblastic leukemia in adults. J Clin Oncol 2017;35:394–401.
18. Walker BA, He J, Chavan SS, Tytarenko R, Zhong S, Deshpande S, et al. A Survey of Fusion genes in myeloma identifies kinase domain activation which could be targeted with available treatments. Blood 2016;128:117.
19. Gu TL, Popova L, Reeves C, Nardone J, Macneill J, Rush J, et al. Phosphoproteomic analysis identifies the M0-91 cell line as a cellular model for the study of TEL-TRKC fusion-associated leukemia. Leukemia 2007; 21:563–6.
20. Kralik JM, Kranewitter W, Boesmueller H, Marschon R, Tschurtschenthaler G, Rumpold H, et al. Characterization of a newly identified ETV6-NTRK3 fusion transcript in acute myeloid leukemia. Diagn Pathol 2011;6:19.
21. Forghieri F, Morselli M, Potenza L, Maccaferri M, Pedrazzi L, Paolini A, et al. Chronic eosinophilic leukaemia with ETV6-NTRK3 fusion transcript in an elderly patient affected with pancreatic carcinoma. Eur J Haematol 2011; 86:352–5.
22. Wai DH, Knezevich SR, Lucas T, Jansen B, Kay RJ, Sorensen PH. The ETV6-NTRK3 gene fusion encodes a chimeric protein tyrosine kinase that transforms NIH3T3 cells. Oncogene 2000;19:906–15.
23. Liu Q, Schwaller J, Kutok J, Cain D, Aster JC, Williams IR, et al. Signal transduction and transforming properties of the TEL-TRKC fusions associated with t(12;15)(p13;q25) in congenital fibrosarcoma and acute myelogenous leukemia. EMBO J 2000;19:1827–38.
24. Russell JP, Powell DJ, Cunnane M, Greco A, Portella G, Santoro M, et al. The TRK-T1 fusion protein induces neoplastic transformation of thyroid epithelium. Oncogene 2000;19:5729–35.
25. Li Z, Tognon CE, Godinho FJ, Yasaitis L, Hock H, Herschkowitz JI, et al. ETV6-NTRK3 fusion oncogene initiates breast cancer from committed mammary progenitors via activation of AP1 complex. Cancer Cell 2007; 12:542–58.
26. Ardini E, Menichincheri M, Banfi P, Bosotti R, De Ponti C, Pulci R, et al. Entrectinib, a Pan-TRK, ROS1, and ALK inhibitor with activity in multiple molecularly defined cancer indications. Mol Cancer Ther 2016; 15:1–13.
27. Drilon A, Li G, Dogan S, Gounder M, Shen R, Arcila M, et al. What hides behind the MASC: clinical response and acquired resistance to entrectinib after ETV6-NTRK3 identification in a mammary analogue secretory carcinoma (MASC). Ann Oncol 2016;27:920–6.
28. Wei G, Patel R, Walsh C, Barrera M, Fagan P, Smith K, et al. Entrectinib, a highly potent pan-TRK, ROS1, and ALK inhibitor, has broad-spectrum, histology-agnostic anti-tumor activity in molecularly defined cancers [abstract]. In: Proceedings of the 28th EORTC-NCI-AACR Molecular Targets and Cancer Therapeutics Symposium; 2016 Nov 29–Dec 2; Munich, Germany. Philadelphia (PA): AACR; 2016. Abstract nr 78.
29. Russo M, Misale S, Wei G, Siravegna G, Crisafulli G, Lazzari L, et al. Acquired resistance to the TRK inhibitor entrectinib in colorectal cancer. Cancer Discov 2016;6:36–44.
30. Lee SJ, Li GG, Kim ST, Hong ME, Jang J, Yoon N, et al. NTRK1 rearrangement in colorectal cancer patients: evidence for actionable target using patient-derived tumor cell line. Oncotarget 2015;6:39028–35.
31. Drilon A, Siena S, Ou SI, Patel M, Ahn MJ, Lee J, et al. Safety and antitumor activity of the multitargeted Pan-TRK, ROS1, and ALK inhibitor entrectinib: combined results from two phase I trials (ALKA-372-001 and STARTRK-1). Cancer Discov 2017;7:400–9.
32. Doebele RC, Davis LE, Vaishnavi A, Le AT, Estrada-Bernal A, Keysar S, et al. An oncogenic NTRK fusion in a patient with soft-tissue sarcoma with response to the tropomyosin-related kinase inhibitor LOXO-101. Cancer Discov 2015;5:1049–57.
33. Weiss GJ, Sachdev JC, Infante JR, Mita MM, Natale RB, Arkenau HT, et al. Phase (Ph) 1/2 study of TSR-011, a potent inhibitor of ALK and TRK, including crizotinib-resistant ALK mutations. J Clin Oncol 2014;32 (15_suppl):e19005.
34. Chi HT, Ly BT, Kano Y, Tojo A, Watanabe T, Sato Y. ETV6-NTRK3 as a therapeutic target of small molecule inhibitor PKC412. Biochem Biophys Res Commun 2012;429:87–92.
35. Dobin A, Davis CA, Schlesinger F, Drenkow J, Zaleski C, Jha S, et al. STAR: ultrafast universal RNA-seq aligner. Bioinformatics 2013;29:15–21.
36. Tarasov A, Vilella AJ, Cuppen E, Nijman IJ, Prins P. Sambamba: fast processing of NGS alignment formats. Bioinformatics 2015;31:2032–4.
37. Liao Y, Smyth GK, Shi W. FeatureCounts: an efficient general purpose program for assigning sequence reads to genomic features. Bioinformatics 2014;30:923–30.
38. Haas B, Dobin A, Stransky N, Li B, Yang X, Tickle T, et al. STAR-fusion: fast and accurate fusion transcript detection from RNA-Seq. bioRxiv [Internet] 2017. Available from: http://www.biorxiv.org/content/early/2017/03/24/120295?%3Fcollection=
39. Westerfield M. The zebrafish book. A guide for the laboratory use of zebrafish (*Danio rerio*). 4th edition. Eugene, OR: University of Oregon Press; 2000.
40. Okabe M, Kunieda Y, Shoji M, Nakane S, Kurosawa M, Tanaka J, et al. Megakaryocytic differentiation of a leukemic cell line, MC3, by phorbol ester: Induction of glycoprotein IIb/IIIa and effects on expression of IL-6, IL-6 receptor, mpl and GATA genes. Leuk Res 1995;19;933–43.
41. Murphy DA, Ely HA, Shoemaker R, Boomer A, Culver BP, Hoskins I, et al. Detecting gene rearrangements in patient populations through a 2-step diagnostic test comprised of rapid IHC enrichment followed by sensitive next-generation sequencing. Appl Immunohistochem Mol Morphol 2016;25:513–523.
42. Leeman-Neill RJ, Kelly LM, Liu P, Brenner AV, Little MP, Bogdanova TI, et al. ETV6-NTRK3 is a common chromosomal rearrangement in radiation-associated thyroid cancer. Cancer 2014;120:799–807.
43. Asou H, Tashiro S, Hamamoto K, Otsuji A, Kita K, Kamada N. Establishment of a human acute myeloid leukemia cell line (Kasumi-1) with 8;21 chromosome translocation. Blood 1991;77:2031–6.
44. Lin J, Zhang W, Zhao JJ, Kwart AH, Yang C, Ma D, et al. A clinically relevant in vivo zebrafish model of human multiple myeloma to study preclinical therapeutic efficacy. Blood 2016;128:249LP-252.
45. The Cancer Genome Atlas Research Network. Genomic and epigenomic landscapes of adult de novo acute myeloid leukemia. N Engl J Med 2013;368:2059–74.
46. Fagan PC, Barrera M, Walsh C, Murphy D, Silverman I, Robert, et al. Antitumor activity of entrectinib, a highly potent pan-TRK, ROS1 and ALK inhibitor, in molecularly defned acute myeloid leukemia [abstract]. In: Proceedings of the American Association for Cancer Research Annual Meeting; 2017 Apr 1–5; Washington, DC. Philadelphia (PA): AACR; 2017. Abstract nr 5158.
47. Nasr R, Lallemand-Breitenbach V, Zhu J, Guillemin MC, De Thé H. Therapy-induced PML/RARA proteolysis and acute promyelocytic leukemia cure. Clin Cancer Res 2009;15:6321–6.
48. Dauvois S, Danielian PS, White R, Parker MG. Antiestrogen ICI 164,384 reduces cellular estrogen receptor content by increasing its turnover. Proc Natl Acad Sci U S A 1992;89:4037–41.

Published OnlineFirst December 13, 2017; DOI: 10.1158/1535-7163.MCT-17-0419

AACR American Association for Cancer Research

Molecular Cancer Therapeutics

Antitumor Activity of Entrectinib, a Pan-TRK, ROS1, and ALK Inhibitor, in *ETV6-NTRK3*–Positive Acute Myeloid Leukemia

Kristen M. Smith, Patrick C. Fagan, Elena Pomari, et al.

Mol Cancer Ther 2018;17:455-463. Published OnlineFirst December 13, 2017.